Homogenization Based Topology Optimization of Fluid-Pressure Loaded Structures using the Biot-Darcy Model

Godfred O. Agyekum, Laurent Cangémi, François Jouve

Homogenization Based Topology Optimization of Fluid-Pressure Loaded Structures using the Biot-Darcy Model

Godfred Oheneba Agyekum[1*], Laurent Cangémi[1†] and François Jouve[2†]

[1*]IFP Energies nouvelles, Rueil-Malmaison, 92852, France.
[2]Université Paris Cité, Laboratoire Jacques-Louis Lions (LJLL), Paris, F-75006, France.

*Corresponding author(s). E-mail(s): godfred.a.o.ezail@gmail.com;
Contributing authors: laurent.cangemi@ifpen.fr; francois.jouve@u-paris.fr ;
†These authors contributed equally to this work.

Abstract

The ambition to develop simulation methods making it possible to predict the integrity or the properties of use (mechanical, diffusive, thermal, electromagnetic, vibratory, etc.) of structures (industrial or natural), materials or processes involved in the development of new advanced technologies is growing consistently. In a global context of permanent development of advanced technologies (notably in the field of energy) and a growing need for cost reduction, the development times for new concepts are increasingly reduced and therefore tend to exclude monolithic design of multiphysic structures. Here, we propose an homogenization based topology optimization method to design multi-scale and multi-physic structures experiencing fluid-pressure loads. Its effect is to allow for micro-perforated composite as admissible designs, where the design is characterized by the material density and its homogenized Hooke's law at each point of the working space, yielding composite designs made of fine mixture between the solid and void phases. The fluid-pressure loads is determined using Biot-Darcy's law and solved using the finite element method. This approach permits a computationally low cost of evaluation of of load sensitivities using the Lagrangian method. As no

assumption is impose on the number of micro-perforation inside the solid domain, this method can be seen as a topology optimization algorithm. We seek minimizers of the elastic compliances, fluid-elastic compliances and of the weight of a solid structure under fluid-pressure loads.

Keywords: Topology optimization, multi-scale, relaxed formulation, theory of homogenization, porous medium, adjoint methods, fluid-structure interaction.

1 Introduction

Shape and topology optimization (or layout optimization) is a popular computational method in structural design and a well developed field with many methods, where most have reached a mature state. Moreover, their ability as design tools to optimize one or more physics continues to grow. Indeed, in all design of multi-scale and multiphysic systems, one of the main challenges to make topology optimization applicable in a large number of advanced technologies is the need to address the inherent multiphysics aspects, such as, the physical mechanisms underlying the behavior of fluids and solids, namely, determining the relationship between fluid-pressure loads and design variables, identifying the boundary to apply the fluid-pressure loads or to effectively assess computationally the sensitivity of such loads, which must very often be taken into account simultaneously during the topology optimization. Among these new advanced technologies, a problem that is currently attracting many attention lies in the design of the heat exchangers [1–6], for various applications such as hot and cold fluids loaded and mechanical structures (e.g., combustion engines, air conditioning, power production or microturbines). Naturally, various additional multiphysics design constraints come into play, such as the need to control the pressure drop induced by the system on the inlet fluid or the mechanical stiffness of the entire structure under fluid-pressure loads. Thus, the performance of the optimized structures is related to the coupled volume forces, induced by the fluid-pressure loads. In the paper, we aim topology optimization by homogenization method to address the announced challenges in the design of multi-scale and multiphysic systems experiencing fluid-pressure loads for a given weight of the solid. Its effect is to allow composite periodically perforated as admissible designs. A key problem characteristic is that, one can easily imagine that even better performance could be achieved through homogenization based topology optimization, since it could make it possible to seek new innovative designs among sets of much freer forms. The main application of our work is the optimization of architectured materials, also known as lattice materials which are becoming increasingly popular in the context of additive manufacturing. In the following, brief history of optimization methods applied to two or more physics problems is introduced.

Hammer and Olhoff in [1], employed topology optimization method to design pressure loaded structure and since been followed by numerous methods to treat such loads in topology optimization setting, such as: (*i*) the boundary variation methods [1, 7–11], (*ii*) the level set methods [6, 12–14], (*iii*) and density based approaches [15–19, 44]. Shape optimization can be divided into two main families: the boundary variation method (or sizing) and the topology optimization (or layout optimization). The boundary variation method is based on *a priori* chosen curves or surfaces, which are used to interpolate the set of admissible boundaries of a given initial design, explicitly captured on a mesh with a fixed topology. Hammer and Olhoff [1] employed the iso-density method to determined the pressure loading boundaries, where Bézier spline curves were used to interpolate the set of admissible boundary shapes. But, Du and Olhoff [7] demonstrated that, the iso-density approach can provide isolines and separate isolines. Furthermore, to employed the iso-density method, one needs to define a starting point and ending points *a priori*, for the pressure loading boundary. Thus, Du and Olhoff [1, 7] introduced a modified isolines method to circumvent these issues. They employed a sensitivity analysis using an efficient finite difference formulation to treat the pressure loading boundaries with respect to design variables. Lee and Martins [9], proposed a novel isolines approach, where there is no need to provide a starting and ending points, combine with an analytical method to calculate the load sensitivities. But, in all the proposed sensitivities evaluation provided by Du and Olhoff, and Lee and Martins [1, 7, 9] were confined to only the exposed pressure loading boundaries. The reader is referred to [8, 11], for more methods dealing with pressure loading boundaries. Moreover, the sensitivity analysis (with respect to design variables) proposed in [1] vanishes or can be disregarded, if the exposed pressure loading boundary coincides with the edges of the finite elements. Note that, the above methods to compute sensitivity analysis are restricted to only boundary motion and do not account for their topology optimization. We emphasize that load sensitivities affect the topology of the result in the design of multiphysic systems and thus, considering load sensitivities in fluid-structure interaction problems is a key characteristic to the performance of an optimal candidate. Therefore, it is necessary to provide a topology optimization algorithm where the sensitivity analysis can be simple to compute, implement and computationally inexpensive.

In [6], a level-set-based approach is used to treat fluid loaded boundary, where in contrast to the boundary variation method, the initial design is implicitly captured on fixed mesh and the topology optimization is performed using simultaneously a level method and the boundary variation of method of Hadamard. In addition, Gao et al. [12] employed a level set function to capture implicitly the structural topology and employed an efficient and robust way to interpolate the set of admissible pressure loading boundary curves. Xia et al. [14], proposed two zero-level sets function, to implicitly captured the free boundary and the pressure loading boundary separately. In [20] (2016), proposed the Distance Regularized Level Set Evolution (DRLSE) (see [13], 2010)

to determine the structural boundary; zero level contour was employed the capture implicitly the loading boundary but did not account for load sensitivities. Recently, Feppon et al. [6] (2018), employed a Level Set Mesh Evolution (LSME) to locate the structural boundary. They used Hadamard's method of shape differentiation to solve a coupled thermal fluid-structure problems. Moreover, Picelli et al. [21] (2019) employed the Laplace's equation to determine hydrostatic fluid pressure fields, in combine with boundary description based on a flood fill procedure: the sensitivity analysis is performed in combination with ersatz material interpolation method. Unfortunately, the above methods tend to be more dependent on the initial design, namely, the boundary variation method or the level set methods provides an optimal solution which is only the best optimum for a given the initial design. Thus, formulate the design problems in terms of optimal distribution of material density is another alternative to performed topology optimization, where there is no need to describe or track the boundary motions. Chen and Kikuchi [44] (2001) introduced a novel approach, wherein, they employed a fictitious thermal loading to solve fluid-structure interaction problems. In addition, Sigmund and Clausen [17] (2007), proposed a mixed displacement-pressure formulation using the finite element method in conjunction with three-phase material (fluid/void/-solid). The given design problem is submitted to a volume constraint on the fluid phase, where, an addition (compressible) void phase is given and also, the mixed finite element methods have to satisfy the Babuška–Brezzi condition to ensure the stability of the element formulation. Moreover, Bourdin and Chambolle [15] (2003), proposed a three-phase material to treat such design problems. Zheng et al. [11] employed a pseudo electric potential to determine the evolving structural boundaries; in their proposed method, the pressure loads were prescribed upon the edges of finite elements, wherein, sensitivity analysis were not performed. For this latter, extra physical fields or phases are often proposed to treat the pressure loading. Recently, Kumar et al [23] (2020), employed similar strategy based on Darcy's law, to design both structures and compliant mechanisms loaded by design-dependent pressure loads using density-based topology optimization. In addition, D. Hübner et al. [24] (2019), employed similar strategy based on Biot model derived by the homogenization of two decoupled problems: (i) deformation of a porous solid saturated by a slightly compressible static fluid and (ii) Stokes flow through the rigid porous structure. The effective medium properties are given by the drained skeleton elasticity, the Biot stress coupling, the Biot compressibility coefficients, and by the hydraulic permeability of the Darcy flow model. This present paper follows a similar strategy based on Biot-Darcy's law to optimize a relaxed (or homogenized) formulation of the original optimization problem to provide a continuous and consistent treatment of composite designs under fluid-pressure loads, which has not been reported before. Our motivation originates from the observation that many industrial applications in the field of energy involve multi-scale designs. We propose a new computational algorithm for two dimensional shape optimization that takes full advantage of a class of periodically

perforated composite to design fluid-pressure loaded structures. The proposed method uses Biot-Darcy's law to characterized the pressure loads and the problem is solved using standard finite elements method. The determined pressure field is then weakly coupled to poro-linear elasticity problem. Herein, we propose an alternate minimization algorithm to treat composite designs under fluid-pressure loads and submitted to volume constraints. The method offers a straightforward computation of loads sensitivities.
In terms of applications, topology optimization has thus far focused on compliance minimization problems and this work should be approached within such background. Furthermore, from a fluid point of view, we emphasize that there exist several homogenized models depending on various scaling regimes assumed by the microstructure pattern (i.e., Darcy, Brinkman, or Stokes regimes, etc.), which makes it unclear which effective model should be used to describe a context featuring all possible regimes simultaneously at different locations in the domain. Thus, in our method, we present a preliminary approach to rigorously treat pressure-loaded microstructures, which suggests the novel potentiality of the method.

In Section 2, we briefly present the original shape optimization problem and its assumed relaxed formulation (introduced in [25]). Next, in Section 3, we present the homogenized fluid-structure models using Biot-Darcy model. Then, in Section 4, we introduce the topology optimization problem formulation for fluid-pressure loaded structures and small-strains, and the associated sensitivity analysis. In Section 5, we present the TO process: it is an alternate direction algorithm, which successively computes the stress field through the solving of a coupled fluid-structure problem over the set of composites periodically perforated by hexagonal cells in 2-d. Finally, in Section 6, we present our numerical results: 2-d computations are displayed of various benchmark design problems involving fluid-pressure loaded structures and small deformation.

2 The original optimal design problem and its relaxed formulation

This section is essentially composed of reminders of existing results in homogenization based shape optimization of elastic structures. An adequate class of admissible designs is introduced which is precisely the concern of the theory of homogenization. Herein, the aim is to devise the least compliant structure compatible with the loads for a given weight of the structure, i.e., to maximize the rigidity of an elastic structure under a weight constraint. We content ourselves to recall the main results detailed in [25], by Allaire, Bonnetier, Francfort and Jouve. These results will be useful for a good understanding of various related subjects that we will be discuss hereafter. The complete proof sometimes very technical can be found in [25].

Let $\Omega \subset \mathbb{R}^N$ be a bounded domain, submit to "smooth enough" mechanical load f, e.g.: $f \in H^{-1/2}(\partial\Omega)^N$, satisfying a Dirichlet boundary condition of

equilibrium on the boundary $\partial\Omega$. Suppose a part of Ω is filled with an isotropic linearly elastic material, with elasticity:

$$A = (\kappa - \frac{2\mu}{N})I_N \otimes I_N + 2\mu I_{2N}, \quad 0 < \kappa, \mu < +\infty, \tag{1}$$

while the other part of Ω is void. Let Ω_χ, denote the subdomain of Ω occupied by the elastic material, where χ is the characteristic function of the solid part in Ω, i.e.,:

$$\chi = \begin{cases} 1 & \text{if } x \in \Omega_\chi \\ 0 & \text{if } x \in \Omega \backslash \Omega_\chi \end{cases} \tag{2}$$

Assume that, Ω_χ is smooth enough open subdomain of Ω, such that f is not zero on $\partial\Omega_\chi \cap \partial\Omega$, i.e., $\partial\Omega_\chi$ contains the part of $\partial\Omega$ where f is not zero, then the following elasticity problem:

$$\begin{cases} \sigma = Ae(u) \quad e(u) = \frac{1}{2}(\nabla u + \nabla^t u), \\ div(\sigma) = 0 \quad \text{in } \Omega_\chi, \\ \sigma \,.\, n = f \quad \text{on } \partial\Omega_\chi \cap \partial\Omega, \\ \sigma \,.\, n = 0 \quad \text{on } \partial\Omega_\chi \setminus \partial\Omega. \end{cases} \tag{3}$$

is well-posed in Ω_χ and has a unique solution $u \in H^1(\Omega_\chi)^N$ (up to a constant function). Wherein, u, σ represent the displacement vector and the associated Cauchy stress tensor (in $L^2(\Omega_\chi;\ \mathbb{R}_s^{N^2})$), respectively. Hence, σ is uniquely defined in $L^2(\Omega;\ \mathbb{R}_s^{N^2})$, for all points $x\Omega$. Thus, σ minimizes the complementary energy, that is:

$$c(\chi) := \int_\Omega A^{-1}\sigma \,.\, \sigma \, dx = \min_{\tau \in \Sigma(\chi)} \int_\Omega A^{-1}\tau \,.\, \tau \, dx, \tag{4}$$

over all statically admissible stress fields, where the set $\Sigma(\chi)$ is defined as fellow:

$$\Sigma(\chi) = \Big\{ \tau \in L^2(\Omega;\ \mathbb{R}_s^{N^2}) \mid div(\tau) = 0 \text{ in } \Omega;\ \ \tau \,.\, n = f \text{ on } \partial\Omega; \\ \tau(x) = 0 \text{ a.e. where } \chi(x) = 0 \Big\} \tag{5}$$

The scalar value $c(\chi)$, defined by (4), is termed the compliance of the body and by performing an integration by parts, we get that

$$c(\chi) = \int_{\partial\Omega} f \,.\, u \, dx,$$

where u is the solution of the linear elasticity problem (3).
Assume that, $\chi(x)$ is the characteristic function of an arbitrary measurable subset of Ω (not necessarily open), then the existence of solution of system (3)

is no longer assured, i.e., σ is no longer guaranteed. However, a generalized compliance can be defined as:

$$c(\chi) := \inf_{\tau \in \Sigma(\chi)} \int_\Omega A^{-1}\tau \,.\, \tau \; dx, \tag{6}$$

where the set $\Sigma(\chi)$ is defined by (5) and wherein, the infimum is not necessarily achieved. Here, the aim is to minimize the compliance of the solid structure under mechanical loads for a given weight of the structure. Thus, the quantity $c(\chi)$ for all characteristic functions χ such that:

$$\int_\Omega \chi(x) \; dx = \Theta, \quad 0 < \Theta \leq |\Omega|,$$

is studied and the minimum compliance reads as:

$$I := \inf \Big\{ c(\chi) \mid \chi \in L^\infty(\Omega;\, \{0,1\}); \quad \int_\Omega \chi(x) \; dx = \Theta \Big\}. \tag{7}$$

The minimum compliance problem defined in (7) is difficult to solve since it is submitted to a volume constraint, that is:

$$\int_\Omega \chi(x) \; dx = \Theta. \tag{8}$$

Such a constraint is usually handled using elementary calculus of variations, namely, by dichotomy process over a positive Lagrange multiplier. Thus, (7) is replaced by:

$$I(\ell) := \inf_{\chi \in L^\infty(\Omega;\, \{0,1\})} \Big\{ c(\chi) + \ell \int_\Omega \chi(x) \; dx \Big\}, \tag{9}$$

where, an elementary calculus of variations is performed in hope to find a positive value ℓ for which the volume constraint (8) is met, which is not so obvious and should be proved. Unfortunately, we do not a proof as detailed in [25], so for the remainder of this paper, the original optimization problem is replaced with the above unconstrained version.

Remark 1 As in [25], we only consider the case where surface loads are applied, for sake of simplicity. However, the model can easily be modified in order to get volume forces or the clamping of part of the boundary $\partial\Omega$. The reader is referred to the numerical examples presented in Sect. 6, which include different types of boundary conditions. The above optimization problem is commonly known as a "single load" problem, i.e., the compliance minimization problem is optimized for a single loading forces and may not be compatible for other loads. Thus, one needs to investigate "multiple loads" problem which amounts to an optimization problem for several configurations, i.e., assume that, $f_1, ..., f_p$ are some given surface loadings and consider

the following minimization problem:

$$I_p(\ell) := \inf_{\chi \in L^\infty(\Omega;\, \{0,1\})} \Big\{ \sum_{i=1}^{p} c_i(\chi) + \ell \int_\Omega \chi(x) \Big\}, \tag{10}$$

where $c_i(\chi)$ is the generalized compliance defined by (6) for the surface load f_i.

It is proved in [26] that problems of the type (7) or (9) do not in general, admit solution, namely, solutions do not exist among characteristic functions. Thus, we must relaxed the problem, i.e., the set of admissible designs must include micro-perforated composite designs. This is because composite designs can always outperform black and white designs, namely, genuine designs made of plain material.
A composite design is described by the local density $\theta(x) \in L^\infty(\Omega;\ [0,1])$ of material and an homogenized elasticity tensor $A^*(x)$ that depends on the microstructure at each point $x \in \Omega$. The homogenized or macroscopic displacement u^* of the structure is then solution of the following set of equations:

$$\begin{cases} \sigma = A^* e(u^*) \quad e(u^*) = \frac{1}{2}(\nabla u^* + \nabla^t u^*), \\ div(\sigma) = 0 \quad \text{in } \Omega, \\ \sigma \,.\, n = f \quad \text{on } \Gamma_N, \\ \sigma \,.\, n = 0 \quad \text{on } \partial\Omega \setminus \Gamma_N, \end{cases} \tag{11}$$

such that Γ_N contains the part of $\partial\Omega$ where f is non zero. Note that, the problem is now defined on the whole working domain Ω and no longer on a design Ω_χ. Thus, the minimization problem defined by (9) is replaced by:

$$I^*(\ell) := \min_{\tau \in \Sigma(\Omega)} \Big\{ \min_{0 \le \theta \le 1} \Big\{ c^*(\theta) + \ell \int_\Omega \theta \, dx \Big\} \Big\}, \tag{12}$$

where $\Sigma(\Omega)$ is defined by:

$$\Sigma(\Omega) = \Big\{ \tau \in L^2(\Omega;\ \mathbb{R}_s^{N^2}) \mid div(\tau) = 0 \text{ in } \Omega;\ \ \tau \,.\, n = f \text{ on } \partial\Omega \Big\}. \tag{13}$$

and $c^*(\theta)$ is defined by:

$$c^*(\theta) = \min_{A^*(x) \in G_{\theta(x)}} \int_\Omega A^{*-1}\tau \,.\tau \, dx, \tag{14}$$

where $G_{\theta(x)}$ is the set of effective or homogenized Hooke's laws for microstructures of density $\theta(x)$. The quantity $c^*(\theta)$, defined by (14) is termed the relaxed or homogenized compliance for a perforated composite material obtained by mixing the material A with holes in proportions $\theta(x)$ and $1 - \theta(x)$. The main challenges in the homogenized formulation (12) are first, to compute the relaxed compliance $c^*(\theta)$ (which can be different from the original compliance $c(\chi)$), second and the most important is to give a full and explicit description

of the set of admissible Hooke's laws G_θ. Unfortunately, we are helpless in this matter, because the set of effective tensors resulting from the mixture in fixed volume fraction of two elastic materials is unknown for the elasticity case, i.e., for the general case of non-defined underlaying microstructure topologies. This difficulty is bypassed when the objective functional is the compliance functional because its minimum can be computed among a well-known subset of the full set of effective tensors, i.e., that of a sequential laminates: see [25] for details. To circumvent these challenges, we follow the same approach in [27, 28], which is to limit the set of admissible composite designs to microstructures for which the Hooke's law can be numerically computed (e.g.: periodic composites with hexagonal cells).
For the remainder of this paper, we content ourselves with the relaxed version (12) of the original optimization problem (9). As such, we denote by u, the homogenized displacement solution of (11) and we seek minimizers for the optimal composite solution under fluid-pressure loads and with a given weight of an elastic material.

3 The fluid-structure model using Biot-Darcy law

As the topology optimization of composite designs progresses, the material boundary and its topology evolve simultaneously, while the material density is optimally distributed with respect to an objective function under mechanical or fluid loads. As such, identifying the boundary to which apply such loads is not easy task, especially in the initial stage of the optimization. Thus, when designing composite structures under fluid-pressure loads and small strains, it becomes essential to establish a design-dependent and continuous pressure field to help the topology optimization. In addition, using 3-d simulation of the pore-scale flow, Jobic et al. established in [29], that different regimes can co-exist within a foam-like composite and that, these regimes depend on the local Reynolds number. They displayed that, a Darcy regime is established for Reynolds numbers lower than 0.3, while an inertia regime is established for a Reynolds greater than 30, preceded by a transition regime. Here, the complexity of these real flow regimes is not taken into account. We consider in this first approach a flow of the Darcean type. However, it was established in [29] that, a Darcy-Forchheimer type approach makes it possible to account for all possible regimes. Thus, exploring this sophisticated flow law is an obvious line of research for future work.
Here, we propose a Biot-Darcy's law to characterize a density-dependent pressure field p. From a fluid point of view, Darcy's law describes the fluid ability to flow through a porous media such as soil, sandstone or rock, namely, the fluid flow through a unit area is said to be directly proportional to the pressure drop per unit length ∇p and that inversely, the resistance of the porous

medium is proportional to the flow μ ([30]). Mathematically, this is defined by:

$$\mathbf{q} := -\frac{\kappa_f}{\mu_f}\nabla p = -K^*\nabla p, \tag{15}$$

where $\boldsymbol{q}$, κ_f, μ_f, and ∇p characterize the flux (ms^{-1}), permeability (m^2), fluid viscosity ($Nm^{-2}s$) and pressure gradient (Nm^{-3}), respectively. In addition, K^*[1] ($m^4N^{-1}s^{-1}$) is the flow coefficient, which characterizes the fluid ability to flow through a porous medium. In order to smoothly and continuously distribute the pressure drop in fluid domain and differentiate between solid and void phase in the whole domain, the flow coefficient $K^*(\theta(x))$ is defined using a smooth function given by:

$$K^*(\theta(x)) := \min\left(\frac{\epsilon_0 + (1-\epsilon_0)(1-\theta(x))}{\theta(x)}, K_\infty\right), \tag{16}$$

where ϵ_0, K_∞ are given thresholds, i.e., $\epsilon_0 = 10^{-4}$, $K_\infty = 10^3$, respectively. Furthermore, the density-dependent pressure field p is assumed to satisfy a Biot's law defined by:

$$p := Mm - Mbe_{vol}, \tag{17}$$

where M, m and e_{vol} are smooth enough functions related to the material density $\theta(x)$ defined by:

$$m(\theta) := (1-\theta)\rho, \quad M(\theta) := \frac{1-\theta}{\kappa_v} - \frac{b(\theta)-(1-\theta)}{\kappa_s}, \quad e_{vol} := \nabla\,.\,u, \tag{18}$$

where ρ, κ_v, and κ_s represent the density of the flux[2], compressibilty of the void and solid phase, respectively. The coefficient $e_{vol} = div(u)$, denotes a volume variation of the solid phase at each finite element. The parameters M and b are the so called Biot modulus and Biot coefficient. The Biot's law (17) is assumed to be related to Darcy's law (15) by:

$$\boldsymbol{q} := mv_f = -K^*\nabla p, \tag{19}$$

where v_f represents the velocity (ms^{-1}) of the flux. Thus, the above equation 19, allows to renders gradually the pressure drop from the inner pressure boundary $\Gamma^f_{p_{in}}$ to the outer boundary pressure $\Gamma_{p_{out}}$. This penetrating pressure of Biot-Darcy's law, is similar to that introduced in [23], which makes this pressure loading boundary a smeared-out version of an applied pressure load on a sharp boundary. Thus, by summing up the contributions of penetrating loads, we obtain the corresponding loads. Therefore, the local differences in the load application is assumed to bear no significant effect on the global behaviour of the structure, which is in line with the Saint-Venant principle.

[1] $K^* = \frac{\kappa_f}{\mu}$ is called "flow coefficient", however, it is sometimes used in literature with a different meaning.

[2] mass per unit volume of the fluid

In addition to the Biot-Darcy equation (19), we assume that the state equation satisfies the law of conservation of mass in view of incompressible fluid, that is:

$$\frac{\partial m}{\partial t} := -div(\mathbf{q}) = div(K^*\nabla p) \tag{20}$$

Consequently, we derived from the Biot's law (17), the equation:

$$\frac{\partial p}{\partial t} := M(\theta(x))\frac{\partial m}{\partial t} - M(\theta(x))b(\theta(x))\frac{\partial e_{vol}}{\partial t}, \tag{21}$$

Further to Biot-Darcy's law (19), we assume for sake of simplicity that our fluid model is continuous and stationary and satisfies the law of conservation of mass (in view of incompressible fluid) defined by:

$$\frac{\partial m}{\partial t} := -div(\mathbf{q}) = div(K^*\nabla p) = 0 \tag{22}$$

where in the particular case of a porous isotropic medium, the Biot's coefficient $b(\theta)$ is explicitly given by:

$$b(\theta(x)) := 1 - \frac{\kappa_s(\theta(x))}{\kappa}, \tag{23}$$

where, κ and $\kappa_s(\theta(x))$ represent the bulk moduli of the solid phase A and the effective (or homogenized) tensor $A^*(x)$. We emphasize that, $A^*(x)$ tends to A, when $\theta(x)$ tends to 1; thus, $\kappa_s(\theta)$ tends to κ.
This paper should be approached within such background, namely, we assume that our fluid-structure model is defined in the particular case of a porous isotropic medium. In order to discuss the precise mathematical settings of our multiphysic system, we introduce the following spaces of functions defined by:

$$V(\Gamma_D^s) := \{v \in H^1(\Omega)^N \mid v = \mathbf{0}, \text{on } \Gamma_D^s\}, \quad V(\Gamma_D^f) := \{q \in H^1(\Omega) \mid q = 0, \text{on } \Gamma_D^f\}, \tag{24}$$

where Γ_D^s and Γ_D^f represent the homogeneous Dirichlet boundaries for the solid and fluid systems, respectively. We consider the subspace:

$$H^{1/2}(\Gamma_N^s) := \{v|_{\Gamma_N^s} \mid v \in V(\Gamma_D^s)\}, \tag{25}$$

and its dual space $H^{-1/2}(\Gamma_N^s)$. Using the Biot-Darcy's law (22), our fluid model is then defined by:

$$\text{(Biot-Darcy)} \begin{cases} -div(K^*\nabla p) = 0 & \text{in } \Omega, \\ p = p_{in} & \text{on } \Gamma_D^f, \\ \mathbf{q}_\Gamma \,.\, \mathbf{n} = f_f & \text{on } \Gamma_N^f, \\ \mathbf{q}_\Gamma \,.\, \mathbf{n} = 0 & \text{on } \Gamma^f = \partial\Omega\backslash(\Gamma_D^f \cup \Gamma_N^f), \end{cases} \tag{26}$$

where $f_f \in H^{-1/2}(\Gamma_N^f)$ (satisfies a compatibility condition of equilibrium) is the enforcement of flux load on the part of its boundary Γ_N^f, i.e.: the enforcement of a Neumann boundary condition, and p_{in} is the loading pressure on the part of its boundary Γ_D^f, i.e.: the enforcement of a Dirichlet boundary condition. Thus, by a straightforward integration by parts, $p \in V(\Gamma_D^f)$ is the unique solution (up to a constant function) to the variational formulation defined by: $\forall q \in V(\Gamma_D^f)$

$$\int_\Omega K^*(\phi)\nabla p \,.\, \nabla q \; dx - \int_{\Gamma_N^f} f_f \; q \; ds = 0 \tag{27}$$

where K^* is the homogenized permeability. Next, we weakly coupled the solution p of the fluid model (26) to the linear-elasticity problem defined by:

$$\text{(Biot-Coussy)} \begin{cases} -div(\sigma) = -b\nabla p & \text{in } \Omega \\ \sigma \,.\, n = f_s & \text{on } \Gamma_N^s, \\ u = 0 & \text{on } \Gamma_D^s, \\ \sigma \,.\, n = 0 & \text{on } \Gamma^s = \partial\Omega \backslash (\Gamma_N^s \cup \Gamma_D^s), \\ \sigma = A^* e(u) & e(u) = \frac{1}{2}(\nabla u + \nabla^t u), \end{cases} \tag{28}$$

where $u \in V(\Gamma_D^s)$ is the unique solution (up to rigid displacement field). Here u is the homogenized displacement vector and σ is the associated Cauchy stress field. The vector function $f_s \in H^{-1/2}(\Gamma_N^s)$ is the body force applied on its boundary Γ_N^s, with a clamping of part on its boundary Γ_D^s. Wherein, the coupling is weak because the equations are solved consecutively, i.e.: first, the Biot-Darcy model, then the linear poro-elasticity model. Thus, by a straightforward integration by parts, u is the unique solution to the variational formulation defined by: $\forall v \in V(\Gamma_D^s)$

$$\int_\Omega A^* e(u) \,.\, e(v) \; dx - \int_{\Gamma_N^s} f_s \; v \; ds + \int_\Omega b\nabla p \,.\, v \; dx = 0 \tag{29}$$

For the remainder of this paper, we weakly solve the variational formulations of the fluid-structure model equations.

4 Topology optimization problem formulation

Herein, we propose an homogenization method for topology optimization of a coupled fluid-structures built with periodic composite materials, characterized by the local density θ of the material and the associated homogenized Hooke's law A^*, defined at each point $x \in \Omega$ of the working space. As in [28], we restrain our analysis to a simple class of composites in plan setting, i.e., our composite materials are periodically perforated by hexagonal cell in 2-d: a regular unit hexagon perforated by smooth hexagon hole, known as smooth honeycomb. This class of modulated periodic microstructures is known to be isotropic

microstructures (or atleast very close to one); the assumption numerically displayed on Fig. 3.

4.1 The Homogenized Hooke's laws

Let Y be the periodic smooth honeycomb cell, i.e., a regular unit hexagon cell perforated by smooth hexagon hole (see, Fig. 1(a)); it is similar to the classical honeycomb, except that the corners of its interior interface are rounded. Thus, when the material density θ tends to one, the smooth hexagon hole tends to a circle with its diameter going to zero. However, the perforated smooth honeycomb hole can not reach completely void, i.e., θ going to zero is excluded. In addition, unlike the classical honeycomb, the smooth honeycomb is not parametrized using the material density, but a parameter $h \in [0, 1]$, homogeneous to a distance. Furthermore, a h-dependent parametric curve Γ_h is then introduced to design the interface solid/void of the perforated smooth honeycomb. In the following, some notations are introduced before giving its polar equation.
Let $v(t) = (\cos(t), \sin(t))^T$ and n_i, for $i \in \{0, 1, 2\}$ represent the normal vectors of the three diagonals of $Y(h)$, defined by

$$n_0 = \begin{pmatrix} 0 \\ 1 \end{pmatrix}, \quad n_1 = \begin{pmatrix} \frac{\sqrt{3}}{2} \\ \frac{1}{2} \end{pmatrix}, \quad n_2 = \begin{pmatrix} \frac{\sqrt{3}}{2} \\ -\frac{1}{2} \end{pmatrix}. \tag{30}$$

Next, the polar equation of Γ_h is defined by:

$$r(t) = h\frac{\sqrt{3}}{2}\Big(\sum_{i=0}^{2} |v(t) \,.\, n_i|^{k(h)}\Big)^{\frac{-1}{k(h)}} \quad \text{with } t \in [0, 2\pi], \tag{31}$$

where k is positive coefficient, depending on h, that here, we set to $k(h) = 4 + 20h^2$. Note that, h, is homogeneous to a distance, similar to the parameter

$$m = \frac{\sqrt{3}}{2}(1 - \sqrt{1 - \theta}),$$

which denotes the relative width of bars with respect to the size of the periodic cell $Y(h)$. Now, let $\mathcal{H}$ be a a regular unit hexagon, i.e., the set of all points such that, the maximal distance of a point in $\mathcal{H}$ from the three diagonals is equal to $\frac{\sqrt{3}}{2}$. Let $M(r, t)$ be a point, with its polar coordinate denoted by (r, t). Thus, M is a point in $\mathcal{H}$ if and only if, its polar coordinate (r, t) satisfies

$$r \max_i |v(t) \,.\, n_i| = \frac{\sqrt{3}}{2}. \tag{32}$$

Consequently, the polar equation of $\mathcal{H}$ verifies

$$r(t) = \frac{\sqrt{3}}{2}(\max_i |v(t) \,.\, n_i|)^{-1}. \tag{33}$$

In addition, we recall that

$$(\sum_{i=0}^{2} |v(t) \,.\, n_i|^k)^{\frac{-1}{k}} \to_{k\to\infty} \max_i |v(t) \,.\, n_i|. \tag{34}$$

Next, the polar equation of Γ_h is obtained by combining the polar equation of $\mathcal{H}$ and the above limit. The parameter h is added in order to adjust the diameter of its inner hole.

Remark 2 It is known in ([31, 32]), that the smooth honeycomb generate lower local concentration stress compare to the classical one. However, we do not claim that the smooth honeycomb can reach a particular elastic properties. In addition, the structure of the periodic smooth honeycomb as well as its Hooke's law are qualitatively similar to the celebrated Vigdergauz hexagonal cell [33], which is known to generate extreme composite microstructures, namely that, they minimize the energy.

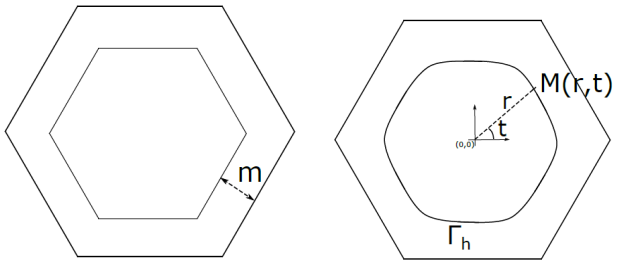

(a) Classical honeycomb (b) Smooth honeycomb

Fig. 1 Isotropic design cells (images taken from [28])

For sake of clarity, few important results on the theory of homogenization are recalled hereafter, the interested reader should refer to textbook [34], for details and explanations.
Assume that, in a given design domain Ω, there is a periodic distribution of holes inside an elastic isotropic phase, with constant elastic tensor A. Let $\epsilon > 0$ be the periodicity size and $Y(h)$ be the rescaled periodicity cell $Y(h)$, i.e., the unit smooth honeycomb. Inside this unit periodic cell, let $Y_0(h)$ be solid part of the subset of $Y(h)$, where its complement being the hole of boundary Γ_h (see, Fig.1(b)). In addition, the porous medium is assumed homogeneous, with an effective tensor $A^*(x)$, whenever ϵ tends to zero.

Now, to compute the homogenized Hooke's law A^*, one needs to solve the cell problems, defined for for each pair $(i,j) \in \{1,2\}$ by:

$$\begin{cases} div(A(e_{ij} + e(w_{ij}))) = 0 & \text{in } Y_0 \\ A(e_{ij} + e(w_{ij})) \,.\, \boldsymbol{n} = 0 & \text{on } \Gamma_h \\ y \mapsto w_{ij}(y) & Y_0 \text{ periodic,} \end{cases} \tag{35}$$

where, w_{ij} is the so-called correctors w_{ij}, corresponding to the local displacements in the periodic cell $Y_0(h)$, and $e_{ij} = \frac{1}{2}(e_i \otimes e_j + e_j \otimes e_i)$, the basis of the symmetric tensors of order 2, with normal to the interior boundary Γ_h denoted $\boldsymbol{n}$. Thus, the variational formulation associated to (35) is defined by: find $w_{ij} \in H^1_{\#}(Y_0, \mathbb{R}^2)$ such that

$$\forall \phi \in H^1_{\#}(Y_0, \mathbb{R}^2) \quad \int_{Y_0} Ae(w_{ij}) \;:\; e(\phi) + \int_{Y_0} Ae_{ij} \;:\; e(\phi) = 0, \tag{36}$$

which admits a unique solution (up to a constant displacement). The coefficients of the homogenized Hooke's law $A^*(x)$ are defined by:

$$A^*_{ijkl} = \frac{1}{\mathsf{Y}} \int_{Y_0} A(e_{ij} + e(w_{ij})) \;:\; (e_{kl} + e(w_{kl}))\, dy \quad \forall i,j,k,l \in \{1,2\} \tag{37}$$

where, the symbol # denotes the periodicity of the correctors w_{ij}, solutions of (36). Note that, one needs to divide the quantity in (37) by the volume $\mathsf{Y}(\mathsf{h})$. Generally, to bypass this point the volume $\mathsf{Y}(\mathsf{h})$ is taken unitary.

Remark 3 It is known that the set Hooke's laws of periodic composites is dense in the set of all possible Hooke's laws reachable with composites [34], thus, restricting the analysis to periodic composites is an acceptable limitation. However, restricting the set of periodic composites to periodically perforated smooth honeycomb is a loss of generality. Hence, Exploring a larger range of periodic microstructures is an obvious line of research for future work.

Since, the smooth honeycomb $Y(h)$ is isotropic cell, we only need for instance two entries of the homogenized tensor A^* (e.g., A^*_{1122} and A^*_{1212}) to fully characterize A^*. However, all the entries of the homogenized tensor A^*, were computed in order to demonstrate that composites periodically perforated by smooth honeycomb are isotropic materials or at least very close to one. For this computation, the range of θ is discretized with 50 triangular elements and A linear material model with Young's modulus $\boldsymbol{E} = 12 \times 10^9 Nm^{-2}$ (i.e., 12GPa) and Poisson's ratio $\nu = 0.35$.

Remark 4 Note that, the void (i.e., $\theta = 0$) is fill with a very compliant material, in order to avoid singularities of the effective tensor when the elasticity problem is solved.

We recall that, the homogenized tensor A^* is isotropic, thus, it is defined as:

$$A^* = 2\mu^* I_{2N} + (\kappa^* - \frac{2\mu^*}{N}) I_N \otimes I_N,$$

where κ^* and μ^* are the bulk and shear moduli of the homogenized Hooke's law A^*, with its Lamé coefficient defined by $\lambda^* = \kappa^* - \frac{2\mu^*}{N}$. In addition, its coefficients are defined by

$$\begin{cases} \mu^* = A^*_{ijij} \\ \lambda^* = A^*_{iijj} \\ \kappa^* = A^*_{iijj} + \frac{2}{N} A^*_{ijij} \end{cases} \qquad \forall i, j \in \{1, ..., N\} \tag{38}$$

Furthermore, the isotropy of the homogenized Hooke's law A^* implies some equalities between its coefficients, i.e.:

$$\forall i, j, k, l, p \in \{1, 2\} \quad \begin{cases} A^*_{iijk} = 0 \\ A^*_{iiii} = A^*_{jjjj} \\ A^*_{iijj} = A^*_{kkll} \\ A^*_{iiii} = A^*_{ijij} + A^*_{llpp} \end{cases} \tag{39}$$

Numerical results

Fig.2 depicts the relative errors to those equalities in (39), computed for discrete sample of material density θ (see, Fig.4). In addition, the homogenized bulk κ^* and shear μ^* moduli of the homogenized Hooke's law A^* were also computed in order to verify that they are bounded by the upper Hashin-Shtrikman bounds, as it is known that any isotropic two-phase composite material is bounded by the Hashin-Shtrikman bounds.

Remark 5 We recall that, the upper Hashin-Shtrikman bounds for the homogenized bulk κ_{HS} and shear μ_{HS} moduli are defined by:

$$\begin{cases} \kappa_{HS} = \frac{\kappa\mu\theta}{\kappa+\mu-\kappa\theta}, \quad \mu_{HS} = \frac{\kappa\mu\theta}{2(\kappa+\mu)-(\kappa+2\mu)\theta} & \text{in 2-D,} \\ \kappa_{HS} = \frac{4\kappa\mu\theta}{3\kappa+4\mu-3\kappa\theta}, \quad \mu_{HS} = \frac{(9\kappa+8\mu)\mu\theta}{5(3\kappa+4\mu)-6(\kappa+2\mu)\theta} & \text{in 3-D} \end{cases} \tag{40}$$

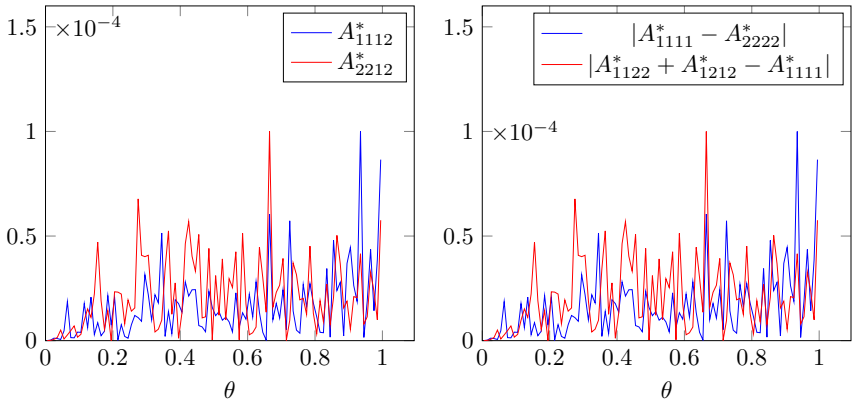

Fig. 2 Isotropy of the smooth honeycomb, i.e.: the maximum residual errors of equalities in 39

In each case, the coefficients are smooth increasing functions with respect to the material density θ, which guarantees that the optimization process will converge. Note that, κ^* and μ^* are closed to the upper Hashin-Shtrikman bounds (see, Fig.3).

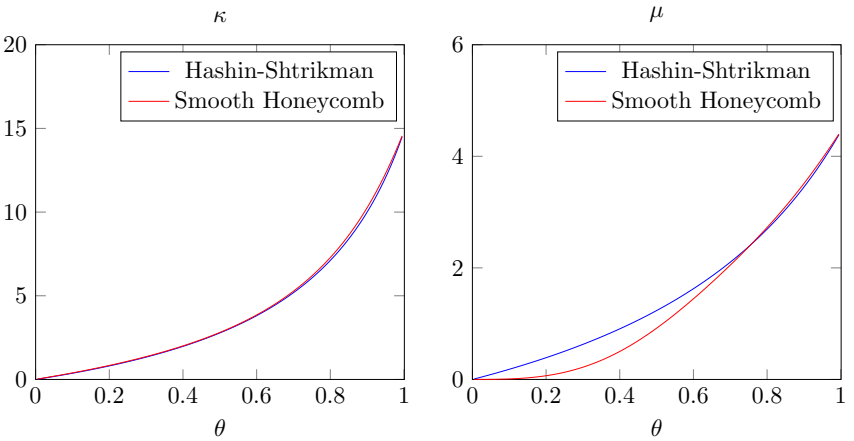

Fig. 3 The bulk κ^* (left) and shear μ^* (right) moduli of the smooth honeycomb wrt. Hashin-Shtrikman bounds

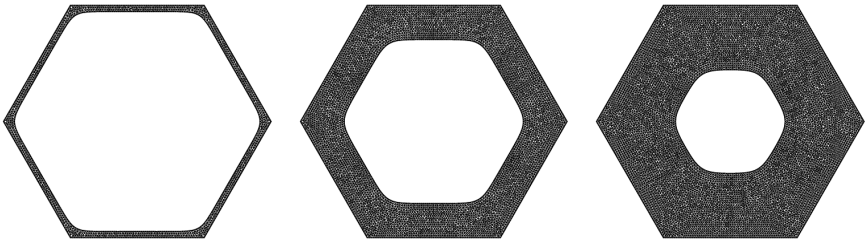

(a) $\theta = 10\%$ (b) $\theta = 50\%$ (c) $\theta = 80\%$

Fig. 4 The Smooth honeycomb cell for different values of to the density θ

4.2 The homogenized conductivity tensor

As in 4.1, starting from a microscopic description of a problem, one seeks a macroscopic or effective model problem in conductivity K^*, we introduce the so-called cell problems and since the considered cell Y is specifically chosen in order to design isotropic composites, only one of its coefficient (e.g., $(K^*)_{11}$) could be computed in order to fully characterized K^*, a scalar value. However to confirm the isotropy, we computed all its coefficients. We denote by $(e_i)_{i=1,2}$ the canonical basis of $\mathbb{R}^2$. For each unit vector e_i, we consider the following conductivity problem in the periodic cell Y:

$$\begin{cases} -div(K(e_i + \nabla w_i))) = 0 & \text{in } Y \\ y \mapsto w_i(y) & Y \text{ periodic,} \end{cases} \tag{41}$$

where $w_i(y)$ is the local variation of pressure created by an averaged (or macroscopic) gradient e_i. The homogenized conductivity tensor K^* is then given in terms of the correctors w_i, solutions of (41), defined by

$$(K^*)_{ij} = \frac{1}{\mathsf{Y}} \int_Y K(e_i + \nabla w_i) \ : \ (e_j + \nabla w_j)\, dy \quad \forall i, j \in \{1, 2\} \tag{42}$$

The constant tensor K^* describes the effective or homogenized properties of the heterogeneous microstructure of periodic size ϵ. Likewise, note that K^* does not depend on the choice of domain Ω, source term f_f, or boundary condition on $\partial\Omega$.

Numerical results

The constant tensor K^* has been computed for the hexagonal cells in 2-d, on the same scheme as the homogenized tensor $A^*(\theta)$ for different values of the density. Figure 5 displays the homogenized flow coefficient K^* computed for a discrete values of the density with respect to the hexagonal cell and normalized smooth function given by (16). As expected, K^* is a decreasing function with respect to the density θ. It is noted that the residual $|(K^*)_{11} - (K^*)_{22}| \leq 10^{-6}$

and $(K^*)_{12} \leq 10^{-3}$, for the hexagonal cell, which validates the isotropy. We emphasize that the flow coefficient K^* can be approximated by the normalized smooth function, that is defined by (16).

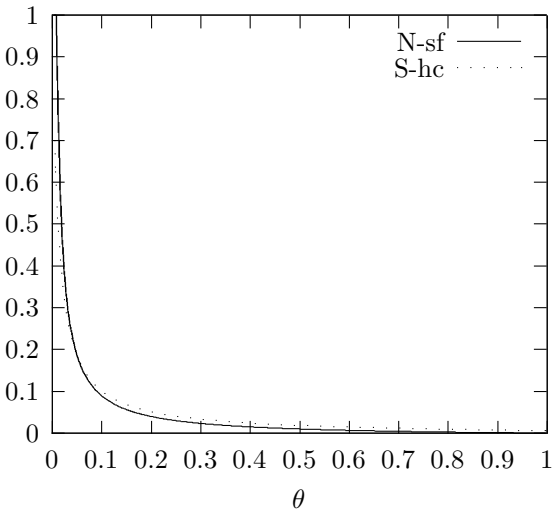

Fig. 5 The homogenized flow coefficient history wrt. the Smooth honeycomb (S-hc) and normalized smooth function (N-sf) in (16)

5 Sensitivity analysis

Here, we present the optimization problem formulation associated to fluidic-pressure loaded structures and discuss the sensitivity analysis for such design problems. The standard formulation, namely the minimization of compliance is considered to design pressure loaded stiff structures, where the optimization problem is given by the constrained formulation:

$$\min_{\substack{0\leq\theta\leq 1 \\ \frac{1}{|\Omega|}\int_\Omega \theta\, dx=\Theta}} \quad c^*(\theta) \tag{43}$$

where $c^*(\theta)$ is the relaxed objective function defined by:

$$c^*(\theta) := \int_{\Gamma_N} f_s \,.\, u\, ds + \int_\Omega (-b\nabla p)\,.\, u\, dx = \min_{\tau\in H_0}\Big\{ \min_{A^*(x)\in G_\theta} \int_\Omega A^{*-1}\tau\,.\tau\, dx\Big\}, \tag{44}$$

with H_0 defined by

$$H_0 = \left\{ \tau\in L^2(\Omega;\, \mathcal{M}_2^s) \mid \begin{cases} -div(\tau - bpI_2) = 0 & \text{in } \Omega \\ \tau\,.\, n = f_s & \text{on } \Gamma_N^s \\ \tau\,.\, n = 0 & \text{on } \Gamma^s \end{cases} \right\} \tag{45}$$

wherein, $\Gamma^s = \partial\Omega\backslash\Gamma_N^s$ is the free part of boundary $\partial\Omega$. We recall that, we only explicitly compute the optimization process on a subset of of all possible Hooke's laws G_θ, i.e.: composites periodically perforated by smooth honeycomb cell. Therefore, the set of effective elasticity tensors $\{A^*(\theta) \mid \theta\in L^\infty(\Omega,[0,1]\}$ has to be characterized. The proposed strategy consists in computing the material properties for a discrete sample of parameter values and using the collected data to construct a surrogate model for the constitutive law (by a simple linear interpolation). Next, the optimization problem (43) is recast as follow:

$$\min_\theta c^*(\theta) = \min_\theta \int_\Omega A^*(\theta)e(u)\ :\ e(u)\, dx, \tag{46}$$

where u is the unique solution to the coupled fluid-elasticity problem given by

$$\begin{cases} (i) & -div(K\nabla p) = 0 \\ (ii) & -div(A^*e(u)) = -b\nabla p \\ (iii) & \frac{1}{|\Omega|}\int_\Omega \theta\, dx = \Theta \end{cases} \tag{47}$$

where Θ is the prescribed volume fraction. Note that, all mechanical equilibrium equations are satisfied under small strain assumption. The optimization problem is then solved using the alternate minimization algorithm [34], which consists in minimizing successively the stress tensor through the solving of the coupled fluid-elasticity problem and then the density θ through a projected

gradient method: it is an algorithm based on *optimality criteria*. We emphasize that, the boundary value problems in (47) are solved in each iteration in combination with the respective boundary conditions.
In a gradient-based topology optimization, it is essential to determine sensitivities of the objective functional and the constraints with respect to the design variable(s). In general, the formulated objective functional depends upon both the state variable u, solution to the mechanical equilibrium equations and the design variable(s). In order to discuss the precise mathematical settings, we introduce the following set of admissible design variables $\mathcal{U}_{ad}$, defined by

$$\mathcal{U}_{ad} := \left\{ \theta(x) \in L^{\infty}(\Omega) \mid \theta(x) \in [0,1], \forall x \in \Omega \right\} \tag{48}$$

We define the applications $\theta \to u(\theta)$, $\theta \to p(\theta)$, where $\theta \in \mathcal{U}_{ad}$ is associated to the solution $\{u(\theta), p(\theta)\} \in V(\Gamma_D^s) \times V(\Gamma_D^f)$ of the state equations (under volume constraints):

$$\begin{cases} (i) & -div(K(\theta)\nabla p) = 0 \\ (ii) & -div(A^*(\theta)e(u)) = -b\nabla p \\ (iii) & \frac{1}{|\Omega|}\int_\Omega \theta \, dx = \Theta \end{cases} \tag{49}$$

As already known [36], the above maps are continuous and differentiable in $\mathcal{U}_{ad}$, where the directional derivative at θ of $u(\theta)$ and $p(\theta)$ with respect to $\bar{\theta} \in L^{\infty}(\Omega)$ are defined respectively by:

$$\left\langle p'(\theta), \bar{\theta} \right\rangle = \bar{p}, \quad \left\langle u'(\theta), \bar{\theta} \right\rangle = \bar{u}, \tag{50}$$

where $\bar{p} \in H_0^1(\Omega)$ and $\bar{u} \in H_0^1(\Omega)^2$ are the unique solutions (up to constant functions) to the system given by:

$$\begin{cases} (i) & -div(K(\theta)\nabla \bar{p}) = div(\bar{K}\nabla p) \\ (ii) & -div(A^*(\theta)e(\bar{u})) = div(\bar{A}^* e(u)) - \bar{b}\nabla p - b\nabla \bar{p}, \end{cases} \tag{51}$$

where

$$\bar{K} =< K'(\theta), \bar{\theta} >, \quad \bar{A}^* =< (A^*)'(\theta), \bar{\theta} > \quad \text{and} \quad \bar{b} =< b'(\theta), \bar{\theta} > \tag{52}$$

represent the directional derivatives at θ with respect to $\bar{\theta}$.

Proof Here, we only give the main results, the reader is referred to [36] for a complete proof. Let $(\theta, \bar{\theta}) \in \mathcal{U}_{ad} \times L^{\infty}(\Omega)$. For all $t > 0$ small enough, $\hat{\theta}(t) = \theta + t\bar{\theta}$ belongs to $\mathcal{U}_{ad}$. Thus, $\hat{p}(t) = p(\hat{\theta}(t))$ and $\hat{u}(t) = u(\hat{\theta}(t))$ are solutions to the system given by:

$$\begin{cases} (i) & -div(\hat{K}(t)\nabla \hat{p}(t)) = 0 \\ (ii) & -div(\hat{A}^*(t)e(\hat{u}(t))) = -\hat{b}(t)\nabla \hat{p}(t) \end{cases} \tag{53}$$

where,

$$\hat{K}(t) = K(\hat{\theta}(t)), \quad \hat{A^*}(t) = A^*(\hat{\theta}(t))$$

We then derive the system (53) with respect to the variable t and the resulting derivatives are evaluated at $t = 0$ in order to get the obtained system (51). □

As already known [36], the objective functional given by:

$$c^*(\theta) = \int_{\Gamma_N} f_s \,.\, u \; ds + \int_\Omega (-b\nabla p) \,.\, u \; dx = \int_{\Gamma_N} j_1(u) \; ds + \int_\Omega j_2(u,p) \; dx \quad (54)$$

is differentiable and the directional derivative at θ with respect to $\bar{\theta}$ is given by:

$$\left\langle c^{*'}(\theta), \bar{\theta} \right\rangle = \int_{\Gamma_N} j_1'(u)\bar{u} \; ds + \int_\Omega \frac{\partial j_2}{\partial u}(u,p)\bar{u} \; dx + \int_\Omega \frac{\partial j_2}{\partial p}(u,p)\bar{p} \; dx \quad (55)$$

wherein, $\bar{p} \in H_0^1(\Omega)$ and $\bar{u} \in H_0^1(\Omega)^2$ are the unique solutions to the equations (51), respectively. Unfortunately, equation (55) is **unusable in practice**, because we cannot deduce a simple expression of the derivative $c^{*'}(\theta)$. Indeed, $\bar{u}$ and $\bar{p}$ are linear functions with respect to $\bar{\theta}$, which are non-explicit. To circumvent this issue, the presented Biot-Darcy-based TO method facilitates use of adjoint-variable method to determine the sensitivities, which is performed using the Céa method.

We introduced the Lagrange multiplier for the constraints (49), associating $\{p(\theta), u(\theta)\}$ to θ, which is $\{\underline{p}, \underline{u}, \ell\} \in H_0^1(\Omega) \times H_0^1(\Omega)^2 \times \mathbb{R}^{*+}$, where ℓ is the Lagrange multiplier designed to respect the volume constraint. In addition, an augmented performance function known as the Lagrangian $\mathcal{L}$ can be defined using the objective function and the mechanical state equations defined by:

$$\begin{aligned} \mathcal{L}(\hat{\theta}, \hat{u}, \underline{\hat{u}}, \hat{p}, \underline{\hat{p}}, \ell) := c^*(\hat{\theta}) &+ \int_\Omega \underline{\hat{u}}(-div(A^*(\hat{\theta})e(\hat{u})) + b(\hat{\theta})\nabla\hat{p}) \; dx \\ &+ \int_\Omega \underline{\hat{p}}(-div(K^*(\hat{\theta})\nabla\hat{p})) \; dx + \ell(\int_\Omega \hat{\theta} \; dx - \Theta), \end{aligned} \quad (56)$$

wherein, $(\hat{\theta}, \hat{u}, \underline{\hat{u}}, \hat{p}, \underline{\hat{p}}) \in L^\infty(\Omega) \times H_0^1(\Omega;\ \mathbb{R}^2)^2 \times H_0^1(\Omega;\ \mathbb{R})^2$ are independent variables. We emphasize that the compliance $c^*(\hat{\theta})$ depends upon the state variables u and p. By straightforward integration by parts, we get

$$\begin{aligned} \mathcal{L}(\hat{\theta}, \hat{u}, \underline{\hat{u}}, \hat{p}, \underline{\hat{p}}, \ell) := c^*(\hat{\theta}) &+ \int_\Omega (A^*(\hat{\theta})e(\hat{u}) \;:\; e(\underline{\hat{u}}) + b(\hat{\theta})\nabla\hat{p} \,.\, \underline{\hat{u}}) \; dx \\ &+ \int_\Omega K^*\nabla\hat{p} \,.\, \nabla\underline{\hat{p}} \; dx + \ell(\int_\Omega \hat{\theta} \; dx - \Theta), \end{aligned} \quad (57)$$

Next, the sensitivities are evaluated by differentiating (57) with respect to u and p in directions $\phi_u \in H^1(\Omega)^2$ and $\phi_p \in H^1(\Omega)$ defined by:

$$\left\langle \frac{\partial \mathcal{L}}{\partial u}(\hat{\theta}, \hat{u}, \underline{\hat{u}}, \hat{p}, \underline{\hat{p}}, \ell), \phi_u \right\rangle = -\int_\Omega b(\hat{\theta}) \nabla p \,.\, \phi_u + \int_\Omega A^*(\hat{\theta}) e(\phi_u) \,:\, e(\underline{\hat{u}})\, dx \quad (58)$$

and

$$\left\langle \frac{\partial \mathcal{L}}{\partial p}(\hat{\theta}, ...,), \phi_p \right\rangle = \int_\Omega (-b \nabla \phi_p) \,.\, u \, dx + \int_\Omega b(\hat{\theta}) \nabla \phi_p \,.\, \underline{\hat{u}} + \int_\Omega K^* \nabla \phi_p \,.\, \nabla \underline{\hat{p}} \, dx \quad (59)$$

which when it vanishes, is nothing more than the variational formulation associated to adjoint-state. Furthermore, the derivatives with respect $\underline{u}$ and $\underline{p}$ in directions $\phi_u \in H^1(\Omega)^2$ and $\phi_p \in H^1(\Omega)$ are simply the state equations defined by:

$$\left\langle \frac{\partial \mathcal{L}}{\partial \underline{u}}(\hat{\theta}, \hat{u}, \underline{\hat{u}}, \hat{p}, \underline{\hat{p}}, \ell), \phi_u \right\rangle = \int_\Omega \Big(A^* e(\hat{u}) \,:\, e(\phi_u)\, dx + b \nabla \hat{p} \,.\, \phi_u \Big), \quad (60)$$

and

$$\left\langle \frac{\partial \mathcal{L}}{\partial \underline{p}}(\hat{\theta}, \hat{u}, \underline{\hat{u}}, \hat{p}, \underline{\hat{p}}, \ell), \phi_p \right\rangle = \int_\Omega K^* \nabla \hat{p} \,.\, \nabla \phi_p \, dx, \quad (61)$$

which when it vanishes, is nothing more than the variational formulation associated to state equations (49). Finally, the partial derivative of the Lagrangian $\mathcal{L}$ with respect to θ in direction $\bar{\theta} \in L^\infty(\Omega;\ \mathbb{R})$ at the stationary point $(u, \underline{u}, p, \underline{p})$ is defined by:

$$\left\langle \frac{d\mathcal{L}}{d\theta}, \bar{\theta} \right\rangle = \int_\Omega \Bigg(- e(u)^T \frac{\partial A^*}{\partial \theta} e(u) + \underbrace{\Big(e(u)^T \frac{\partial A^*}{\partial \theta} e(\underline{u}) + \frac{\partial K^*}{\partial \theta} \nabla p \,.\, \nabla \underline{p} + \frac{\partial b}{\partial \theta} \nabla p \,.\, \underline{u} + \ell \Big)}_{\text{Load sensitivities}} \Bigg) \bar{\theta} \, dx \quad (62)$$

6 Topology optimization over composite materials

6.1 Alternate minimization method

This section presents the proposed numerical algorithm, which is based on the homogenization method. The key idea is to compute composite designs for the relaxed formulation rather than "classical" designs, which are merely approximately optimal for the original formulation. Our optimization problem is solved using the alternative minimization algorithm. We seek minimizers of sum of the elastic compliance, fluid-elastic compliance and of the weight of a solid structure under fluidic pressure loads.

6.1.1 Minimizing over the stress field.

Minimization over the stress field σ consists in solving the linear elasticity problem (28) over the effective tensor $A^*(x)$, for given design $\theta(x)$ of microstructure periodically perforated by the smooth honeycomb cell. Consequently, the linear elasticity problem (28) can be recast as a variational problem defined by:

$$v \in V(\Gamma_D^s), \quad \int_\Omega A^*(\theta)e(u) \ : \ e(v)\ dx = \int_{\Gamma_N^s} f_s\ .v\ ds + \int_\Omega (-b\nabla p)\ .\ v\ dx \quad (63)$$

which numerically is solved using P_1 finite elements to compute the displacement vector field u.

6.1.2 Minimizing over the density field.

Minimization over the density field θ for a given stress tensor σ is performed using the projected gradient algorithm. The minimum compliance problem defined by (44) is not a self-adjoint, hence one needs to define the associated adjoint problem, which we define herein using the Céa method presented in sect.(5). The descend direction $h = d\theta$ is given by solving the bilinear equation:

$$\left\langle \frac{\partial \mathcal{L}}{\partial \theta}, h \right\rangle = -\int_\Omega \Big(e(u)^T \frac{\partial A^*}{\partial \theta} e(u) - \underbrace{\Big(e(u)^T \frac{\partial A^*}{\partial \theta} e(\underline{u}) + \frac{\partial K^*}{\partial \theta} \nabla p\ .\ \nabla \underline{p} + \frac{\partial b}{\partial \theta}(\theta) \nabla p\ .\ \underline{u} + \ell \Big)}_{\text{Load sensitivities}} \Big) h\ dx, \quad (64)$$

where the descend direction $h = d\theta$, has to satisfy the inequality given by:

$$\left\langle \frac{\partial \mathcal{L}}{\partial \theta}(\theta, u, \underline{u}, p, \underline{p}, \ell), d\theta \right\rangle < 0 \quad (65)$$

which is achieved by choosing:

$$d\theta = \left(- e(u)^T \frac{\partial A^*}{\partial \theta} e(u) + \underbrace{\left(e(u)^T \frac{\partial A^*}{\partial \theta} e(\underline{u}) + \frac{\partial K^*}{\partial \theta} \nabla p \,.\, \nabla \underline{p} + \frac{\partial b}{\partial \theta}(\theta) \nabla p \,.\, \underline{u} + \ell \right)}_{\text{Load sensitivities}} \right) \tag{66}$$

At iteration n, the optimal density θ is then updated by performing the projected gradient:

$$\theta^{n+1} = P_{[0,1]}(\theta^n + \delta d\theta), \tag{67}$$

where $\delta > 0$ is the step size and $P_{[0,1]}$ is the projection operator on the interval $[0, 1]$. The value of the Lagrange multiplier ℓ is computed at each iteration by a dichotomy process designed to respect the volume constraint. We emphasize that the exact value of ℓ can not be analytically given because of the projection operator: numerically, the partial derivative of the Lagrangian $\frac{\partial \mathcal{L}}{\partial \theta}$ is regularized using an equivalent H^1-norm by solving the following variational formulation:

$$\int_\Omega (\frac{\partial \mathcal{L}}{\partial \theta} h + \eta^2 \nabla \frac{\partial \mathcal{L}}{\partial \theta} \,.\, \nabla h)\, dx = - \int_\Omega \left(\frac{\partial A^*}{\partial \theta} e(u) \,:\, e(u) - \frac{\partial A^*}{\partial \theta} e(u) \,:\, e(\underline{u}) - \frac{\partial K^*}{\partial \theta} \nabla p \,.\, \nabla \underline{p} - \frac{\partial b}{\partial \theta} \nabla p \,.\, \underline{u} - \ell) \right) h \, dx, \tag{68}$$

where η is a small coefficient, which typically depends on the size of the elements of the mesh: thanks to this coefficient, we are able to numerically regularize the partial derivative on a length scale of order η and to limit the checkerboard effect on the density θ, similar to those reported in [37–39]. In practice, we use an adaptive step size δ, which consists in increasing δ by 20%, if the newly computed homogenized structure is accepted: if current compliance is lower than the previous one, else δ is divided by 2.

6.1.3 Volume constraint.

As explained in sect. 2, we do not known how to determine ℓ beforehand. As such, an alternative computations were performed, where the Lagrange multiplier ℓ is adjusted at each iteration, so that the corresponding value of the optimal density satisfies the volume constraint. In other words, once the stress σ^n is computed through (63), we determine θ^n through (67) and then ℓ^n is determined through a simple iterative procedure, namely by dichotomy.

6.2 Implementation

This section presents our complete optimization process to perform topology optimization of structures under fluidic pressure loads and some general difficulties related to the homogenization method.

6.2.1 Complete optimization algorithm.

The Alternate direction algorithm is an iterative method, structured as follows:

Algorithm 1

---

1. Initialization of the design variable θ such that :

$$\forall x \in \Omega \quad \theta^0(x) = \frac{\Theta}{\int_\Omega 1 \, dx}$$

2. Iteration until convergence, for $n \geq 0$:
   (a) Computation of the state variable p^n through the Biot-Darcy problem (26), with design variable $(\theta^n(x), A^*(x))$
   (b) Computation of the stress tensor σ^n through the linear elasticity problem (28), with design shape $(\theta^n(x), A^*(x))$
   (c) Computation of the descend direction $d\theta^n$ for the stress tensor σ^n using formulas (65-68)
   (d) Updating the design variable θ^{n+1} using formulas (66) for the descend direction $d\theta^n$ and then updating the effective tensor $(\theta^{n+1}(x), A^*(x))$, by linear interpolation.

Note that, the alternate direction algorithm is apparented to the two known methods in [40–42].

6.2.2 Convergence criterion.

The procedure is iterated until the quantity

$$max\left((\max_i(|\theta_i^{n+1} - \theta_i^n|), 1 - \frac{\int_\Omega A^{*-1}(\theta^{n+1})\sigma^{n+1} \ : \ \sigma^{n+1} \, dx + \ell \int_\Omega \theta^{n+1} \, dx}{\int_\Omega A^{*-1}(\theta^n)\sigma^n \ : \ \sigma^n \, dx + \ell \int_\Omega \theta^n \, dx} \right)$$

becomes smaller than a preset threshold. About 100 iterations are required to reach a criterion of order 10^{-5}. Other convergence criteria could be used, for instance the L^2 norm of $\sigma^{n+1} - \sigma^n$.

7 Numerical results and discussion

In the following, we treat a variety of (benchmark) test cases to demonstrate that, our alternate minimization algorithm for topology optimization of coupled fluid-structure problems produces physically correct results, while minimizing the sum of the elastic compliance, fluid-elastic compliance and of the weight of a solid structure. Any change in the value of considered parameters is reported within the definition of the problem formulation. The above

algorithm has been implemented in FreeFem++[43], where all the unknowns are discretized using P_1 finite elements. For all our computations, a linear material model with Young's modulus $\boldsymbol{E} = 12 \times 10^9 Nm^{-2}$ and Poisson's ratio $\nu = 0.35$ are considered. The void (i.e., $\theta = 0$) is replaced with a very compliant material: namely, the smallest admissible value of θ is fixed at $1.e-3$, in order to avoid singularities of the effective tensor when the elasticity problem is solved.

7.1 Pressurized arch

This example was originally introduced and solved in [11, 23]. The structure to be found is rectangle of dimensions $0.2m \times 0.1m$, fixed at the edges of its left and right bottom on a zone of width $\frac{1}{8}$, while submitted to a pressure load $p = 1$ bar (i.e., $1 \times 10^5 Nm^{-2}$) and vanishes on the boundary $\Gamma^f_{p_0}$ (i.e., $p|_{\Gamma^f_{p_0}} = 0$): see Fig.6 for a schematic of this test case. The workspace Ω is discretized with 44492 triangular elements.
On Fig.7, we plot the objective function history for this calculation: smooth and relatively fast convergence is observed; while Fig.8 displays the output of the alternate minimization algorithm for a volume fraction set to $\Theta = 20\%$, with the resulting pressure field, deformed mesh, and von Mises stress at the final state. The density θ is represented with a gray scale: areas where $\theta = 1$ are black (pure material), whereas white regions correspond to voids.
The topology of the result is similar to that obtained in previous literature [23], for similar problems with different design and optimization settings. Although one can guess a "shape" on the edges of the structure, its center contains a large composite zone.

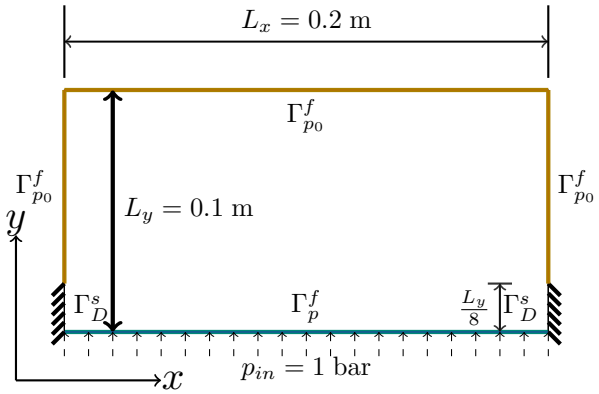

Fig. 6 Setting for fluid-elastic compliance minimization problem of 7.1 issued from [11, 23]

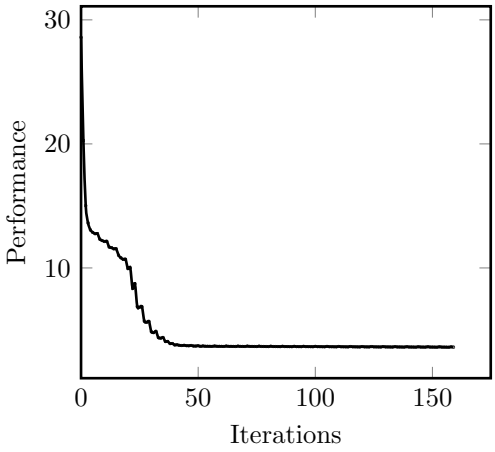

Fig. 7 Convergence history for fluid-elastic compliance minimization problem of Section 7.1

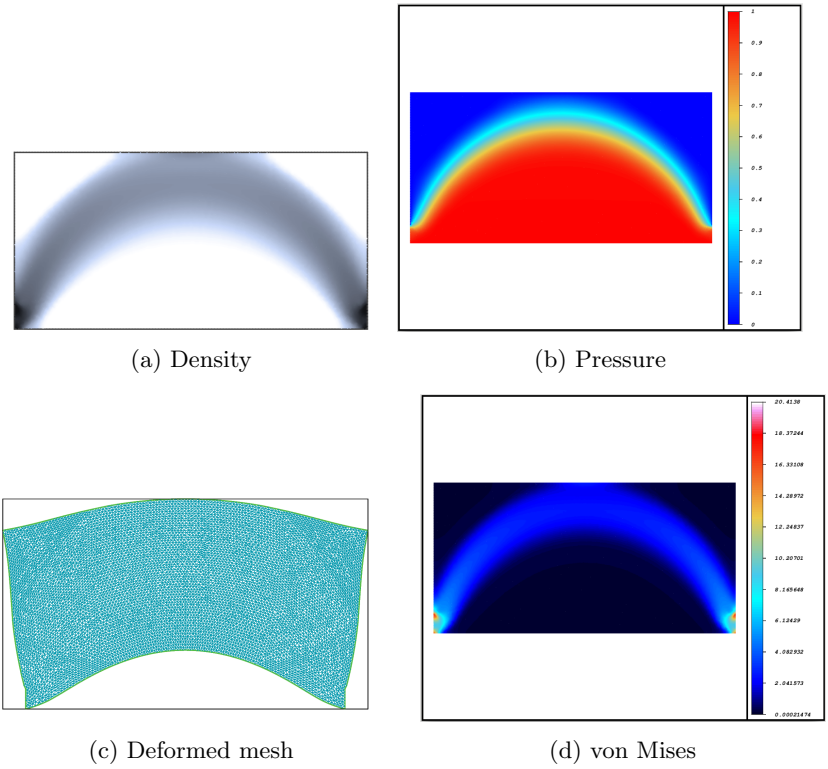

(a) Density (b) Pressure

(c) Deformed mesh (d) von Mises

Fig. 8 (a) The optimal density, (b) pressure field, (c) deformed mesh, and (d) von Mises stress for test case 7.1

7.2 Pressurized piston

This second test case was originally introduced and solved in [15, 23]. The workspace is a $0.12m \times 0.04m$ rectangle, fixed on the boundary Γ_D^s, while submitted to pressure load $p = 1$ bar on the upper boundary Γ_p^f and vanishes on boundary $\Gamma_{p_0}^f$: see Fig.9 for a schematic of this test case. The volume fraction is set to $\Theta = 30\%$. It is desired to find a stiffest optimum design "shape" which can convey the applied pressure loads on the upper boundary to the lower fixed support readily.

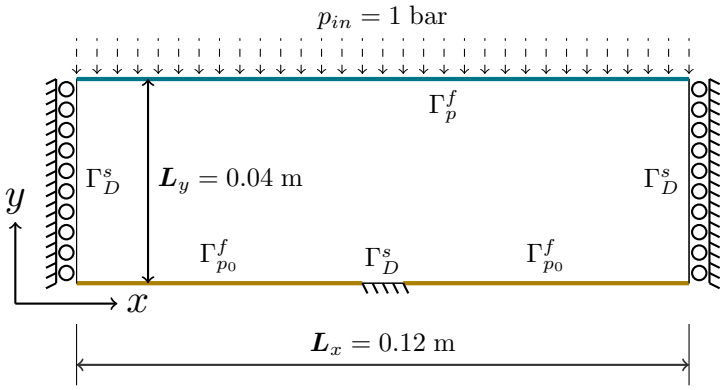

Fig. 9 Setting for fluid-elastic compliance minimization problem of test case 7.1 issued from [15, 23]

On Fig.10, we plot the convergence history for this calculation: smooth and relatively rapid convergence is observed; while Fig.11 depicts the optimal density and the pressure field, deformed mesh, and von Mises stress at final state. The topology of the result is similar to that obtained in previous literature [9, 20, 21, 23], for similar problems with different design and optimization settings. Although one can guess a "shape" on the edges of the structure, its center contains a large composite zone.

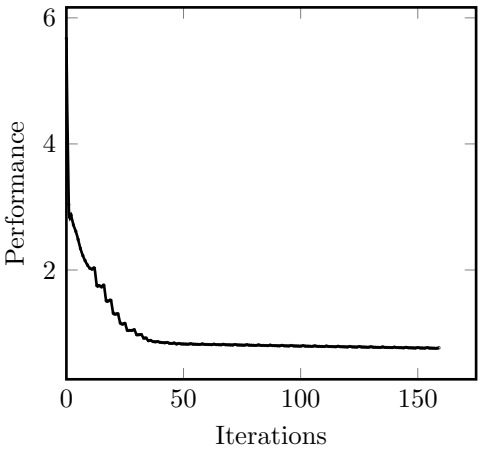

Fig. 10 Convergence history for the fluid-elastic compliance minimization problem of Section 7.2

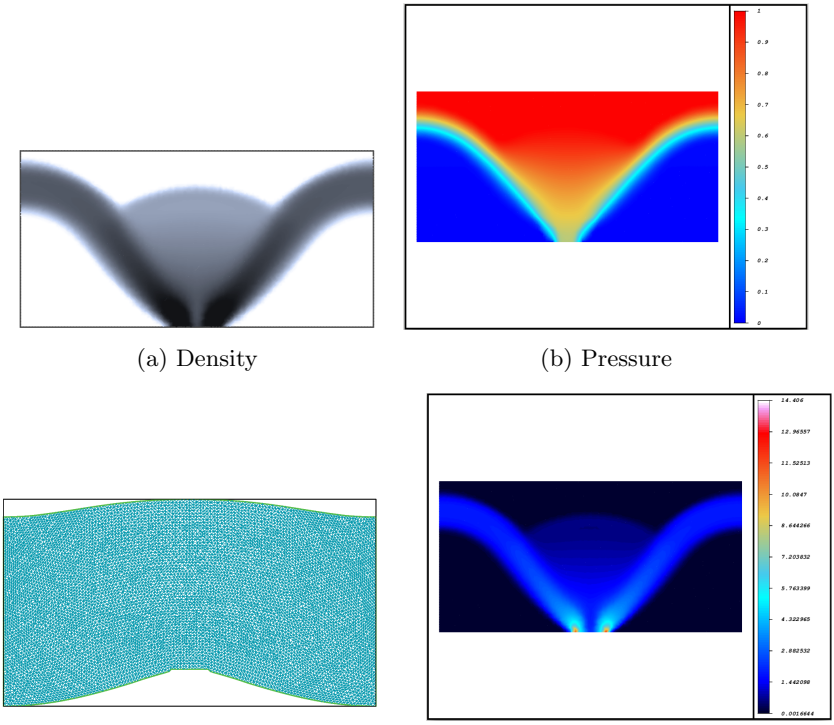

(a) Density (b) Pressure

(c) Deformed mesh (d) von Mises

Fig. 11 (a) The optimal density, (b) pressure field, (c) deformed mesh, and (d) von Mises stress for test case 7.2

7.3 Pressurized MBB

In this test case, the structure to be found is submitted to pressure load $p_{in} = 1$ bar on the boundary Γ_p^f, while its boundary Γ_D^s is clamped. The workspace Ω is sketched on Fig.12: a rectangle of dimensions $0.3m \times 0.1m$. The domain is discretized with 43440 triangular elements, where the volume fraction is set to $\Theta = 30\%$. Note that, this example has already been investigated by several authors in the case of structural design under mechanical loading.

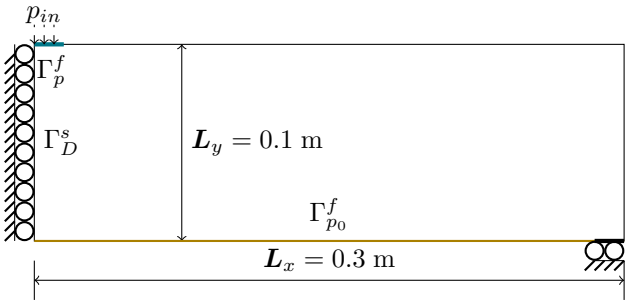

Fig. 12 Setting for fluid-elastic compliance minimization problem of Section 7.3

on Fig.13, we plot the convergence history for this calculation: smooth and relatively fast convergence is observed, while Fig.14 displays the topology of the final design and the resulting von Mises stress, pressure field and deformed mesh under pressure loads at the final state. Very interestingly, we retrieve the fact that the topology of the result is similar to that obtained in the case of mechanical load.

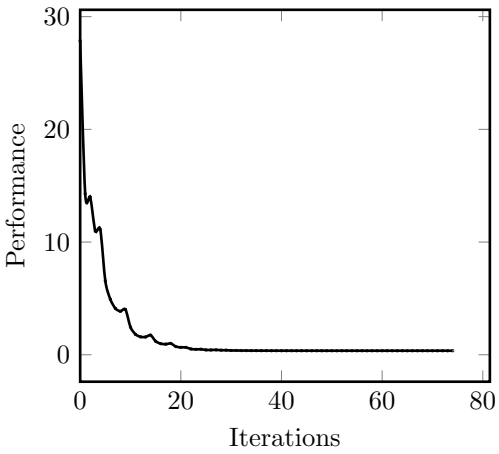

Fig. 13 Convergence history for the fluid-elastic compliance minimization problem of Section 7.3

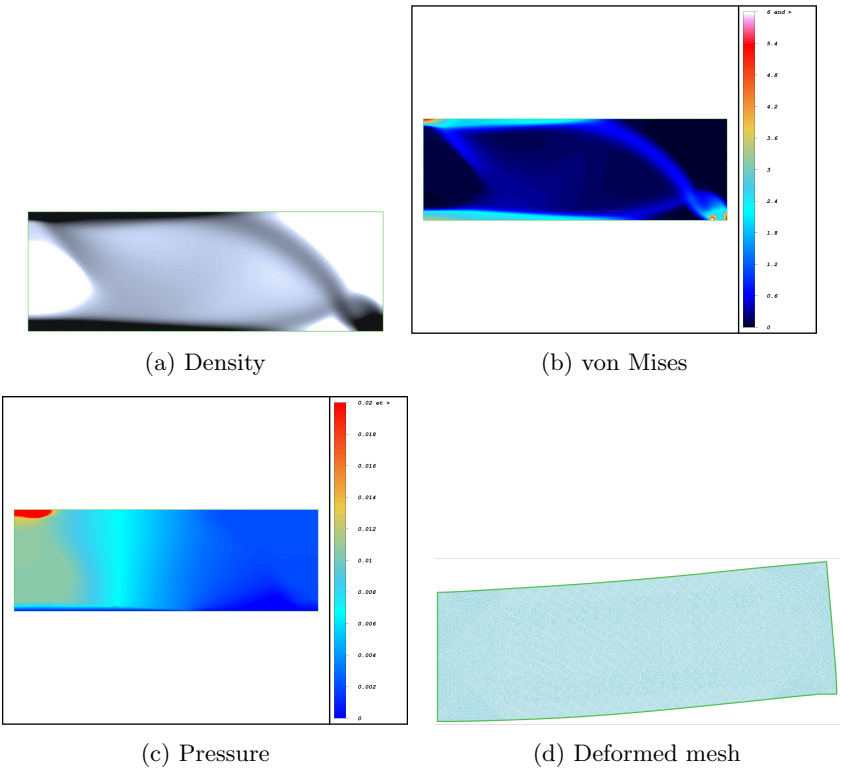

(a) Density (b) von Mises

(c) Pressure (d) Deformed mesh

Fig. 14 (a) The optimal density, (b) von Mises stress, (c) pressure field, and (d) deformed mesh for test case 7.3

7.4 Two dimensional counter-flow exchanger

In this example, the structure to be found is a two-dimensional counter-flow exchanger of dimensions 2×2.2. The setup is seen in Fig.15 and consists of a fluid inlet of density $\boldsymbol{q}_{0,1}$, in the lower-left part of the domain, with the corresponding outlet pressure on the opposite lower-right side; also, another fluid inlet of density $\boldsymbol{q}_{0,2}$ is located at the upper-right side of the domain, with the corresponding outlet pressure at the opposite upper-left side. All the other boundaries in this device are insulated from the outside: zero Neumann boundary conditions hold for the pressure (i.e., $\frac{\partial p}{\partial n} = 0$), while homogeneous Dirichlet boundary conditions are applied on the boundary of a small non optimizable rectangle ω of dimensions 2×0.2. The numerical values of the parameters involved are displayed on Fig.16.

Our aim is to achieve a trade-off between the minimization of the compliance imposed by the fluid and the maximization of the hydraulic strain energy,

subject to the volume constraint (or not), that is:

$$J^*(\theta, u(\theta)) = \alpha \underbrace{\left(\int_\Omega A^* e(u) \, : \, e(u) \, dx \right)}_{\text{Elastic strain energy}} + (1-\alpha) \underbrace{\left(- \int_\Omega K^* \nabla p \, . \, \nabla p \, dx \right)}_{\text{Hydraulic strain energy}}, \quad s.t. \left\{ \frac{1}{|\Omega|} \int_\Omega \theta \, dx = \Theta \right. \tag{69}$$

where $\alpha \in [0,1]$ is termed as a weighting factor: it measures the relative weight given to each term in (69). The objective functional $J^*(\theta, u(\theta))$ corresponds to the internal energy stored inside the structure. Here, we consider to two configurations, i.e.: (i) a test case with volume constraint set to $\Theta = 20\%$, first and (ii) test case without volume constraint, second, for several values of α.

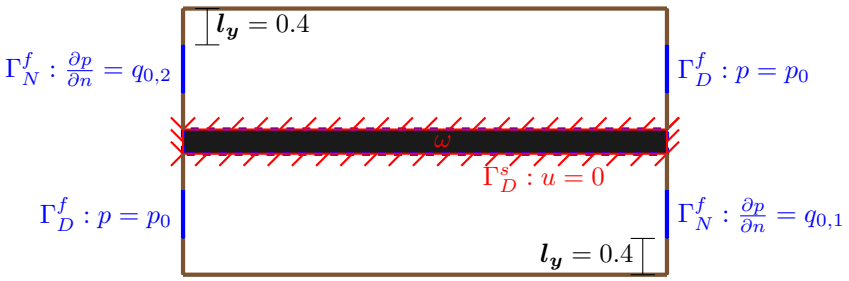

Fig. 15 Setting of the 2-d counter-flow exchanger 7.4. The brown layers at the walls stand for zero Neumann boundary conditions for the pressure (i.e., $\frac{\partial p}{\partial n} = 0$); homogeneous Dirichlet boundary conditions hold on $\partial\omega$.

p_0	$\boldsymbol{q}_{0,1}$	$\boldsymbol{q}_{0,2}$
1.5	3	5

Fig. 16 Numerical values of the physical parameters in the 2-d counter-flow exchanger test case in Section 7.4

Fig. 17 to Fig. 18 display the optimal densities for a sweep of α for the two configurations, i.e.: with or without volume constraint. Very interestingly, we retrieve the fact that the topology of the results contains a large composite zone, where the force contribution induced by the fluid appears in all directions, which evidently, prior to the analysis is expected. For this latter, the corresponding objective history for the two configurations are depicted on Fig. 19 to Fig. 20. On Fig. 21, we plot the final volume with respect to α for the second configuration (i.e.,with volume unconstrained), while on Fig. 22 to Fig. 23,

we show the convergence history for $\alpha = 1/2$ for the both configurations. On Fig. 24, we display the corresponding pressure field for both configurations, with $\alpha = 1/2$.

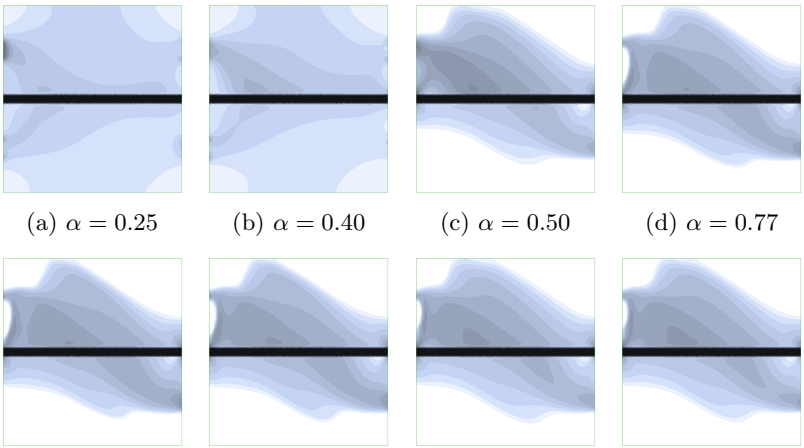

(a) $\alpha = 0.25$ (b) $\alpha = 0.40$ (c) $\alpha = 0.50$ (d) $\alpha = 0.77$

(e) $\alpha = 0.80$ (f) $\alpha = 0.85$ (g) $\alpha = 0.90$ (h) $\alpha = 0.95$

Fig. 17 The Optimal densities for a sweep of α, with volume fraction $\Theta = 20\%$

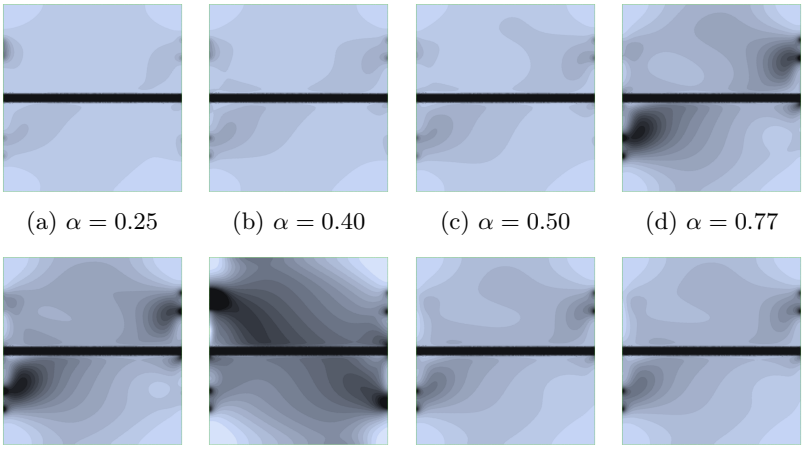

(a) $\alpha = 0.25$ (b) $\alpha = 0.40$ (c) $\alpha = 0.50$ (d) $\alpha = 0.77$

(e) $\alpha = 0.80$ (f) $\alpha = 0.85$ (g) $\alpha = 0.90$ (h) $\alpha = 0.95$

Fig. 18 The Optimal densities for a sweep of α, without volume constraint

α	0.25	0.40	0.50	0.77	0.85	0.90	0.93	0.95
$J^*(\alpha)$	-4.51	-0.06	0.962	5.055	5.025	6.533	10.17	0.163

Fig. 19 The converged objective function wrt. α, with volume fraction $\Theta = 20\%$

α	0.25	0.40	0.50	0.77	0.85	0.90	0.93	0.95
$J^*(\alpha)$	-4.51	-2.54	-1.83	-0.57	-0.55	-1.47	0.026	0.286

Fig. 20 The converged objective function wrt. α, without volume constraint

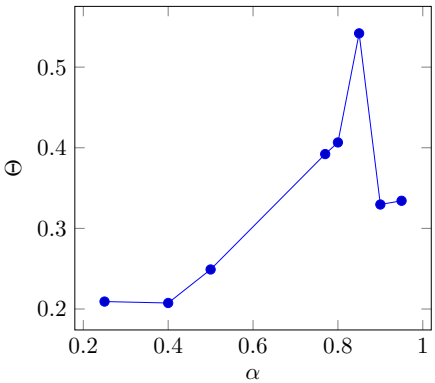

Fig. 21 The final volume history wrt. α, in the second configuration, i.e., without volume constraint.

We note that, in both configurations, namely when the optimization is subjected to a volume constraint or not, the topology of the optimal design is α dependent, namely, for all $\alpha \in (0, 0.40)$, the topology tends to maximize the hydraulic strain energy, which in process minimize the output pressure, whereas for all $\alpha \in [0.40, 1)$, the topology of the result tends to achieve a trade-off between the minimization of the compliance induced by the fluid and the maximization of the hydraulic strain energy, which evidently is what we intent to achieve for this optimization problem. However, in the second configuration (i.e.,without volume constraint), we emphasize a gain of volume fraction but not necessarily a gain in performance, see Fig. 20.

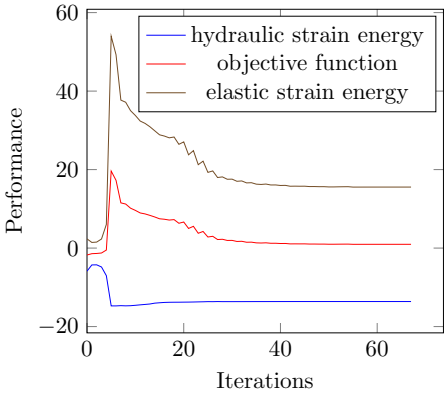

Fig. 22 The convergence history wrt. $\alpha = 1/2$, for volume constraint $\Theta = 20\%$

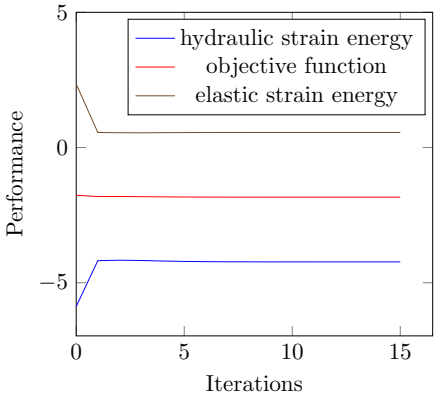

Fig. 23 The convergence history wrt. $\alpha = 1/2$, and with no volume constraint

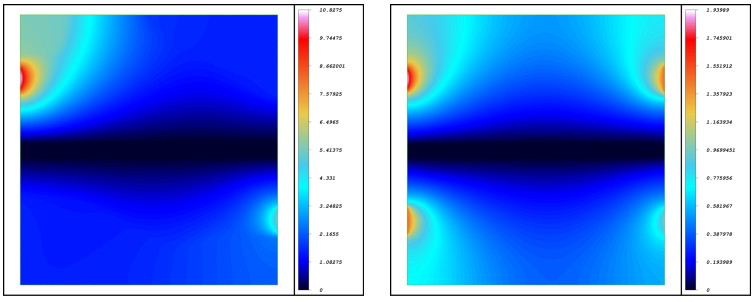

(a) with volume constraint (b) without volume constraint

Fig. 24 The pressure field at final state for both configuration: with and without volume constraint, for $\alpha = 1/2$

8 Conclusion and perspectives

In this paper, we intent to provide a contribution to the understanding and modeling of the physical mechanisms underlying the behavior of fluids and solids (materials and structures) and to deploy a multiphysic and multi-scale analysis of these behaviors. Here, homogenization method is used to perform topology optimization of fluid-pressure loaded structures using Biot-Darcy model, where a standard finite element formulation is employed and does not need explicit description of the pressure loaded boundary. We weakly coupled the fluid-pressure loads inside composite designs periodically perforated by smooth honeycomb cell, yielding isotropic periodic composite designs. As the weakly coupled fluid-pressure loads is density-dependent, it becomes essential to determine the load sensitivities, where herein, a projected gradient method is used. The method facilitates analytical calculation of the load sensitivities with respect to the design variables using the computationally inexpensive adjoint-variable method. This availability of load sensitivities is a key characteristic over many other methods to treat pressure loads in topology optimization. Furthermore, the consideration of load sensitivities within the homogenization approach does affect the topology of the results, thus, the load sensitivities terms are essential to the topology optimization of the multiscale and multiphysic structures. The proposed projected gradient algorithm offers relatively easy extension to 3D problems. The potentiality and robustness of the proposed method is verified by minimizing the sum of the elastic and fluid-elastic compliance, and of the weight of a solid structure under pressure loads. For future work, extension to 3D structures and to liquid-liquid heat exchangers problems are prime directions.

Declarations

On behalf of all authors, the corresponding author states that there is no conflict of interest.

Replication of results

On behalf of all authors, the corresponding author states that there is no codes available as supplementary material because this work is carried out as part of a thesis in partnership with IFPEN. The latter holds the intellectual rights.

References

[1] Hammer, V.B. and Olhoff, N., Topology optimization of continuum structures subjected to pressure loading, J. Structural and Multidisciplinary Optimization, 19(2) (2000) 85-92.

[2] Papazoglou, P., Topology optimization of heat exchangers, TU Delft, (2015).

[3] Pietropaoli, M. and Montomoli, F. and Gaymann, A., Three-dimensional fluid topology optimization for heat transfer, J. Structural and Multidisciplinary Optimization, 59 (2019) 801-812.

[4] Saltzman, D. and Bichnevicius, M. and Lynch, S. and Simpson, T.W. and Reutzel, E.W. and Dickman, C. and Martukanitz, R., Design and evaluation of an additively manufactured aircraft heat exchanger, J. Applied Thermal Engineering, 138 (2018) 254–263.

[5] Saviers, K.R. and Ranjan, R. and Mahmoudi, R., Design and validation of topology optimized heat exchangers, AIAA Scitech 2019 Forum, 1465.

[6] Feppon, F. and Allaire, G. and Bordeu, F. and Cortial, J. and Dapogny, C., Shape Optimization of a Coupled Thermal Fluid-Structure Problem in a Level Set Mesh Evolution Framework, J. Boletin de la Sociedad Española de Matemática Aplicada, Springer 76(3) (2019) 413-458.

[7] Du, J. and Olhoff, N., Topological optimization of continuum structures with design-dependent surface loading - Part I: New computational approach for 2D problems, J. Structural and Multidisciplinary Optimization 27(3) (2004) 151-165.

[8] Fuchs, M.B. and Shemesh, NNY., Density-based topological design of structures subjected to water pressure using a parametric loading surface, J. Structural and Multidisciplinary Optimization, 28(1) (2004) 11-19.

[9] Lee, E. and Martins, JRRA., Structural topology optimization with design-dependent pressure loads., J. Computer Methods in Applied Mechanics and Engineering, 40-48 (2012) 233-236.

[10] Li, Zm and Yu, J. and Xu, L., N., Topology optimization of pressure structures based on regional contour tracking technology, J. Structural and Multidisciplinary Optimization, 58(2) (2018) 687-700.

[11] Zheng, B. and Chang, C.J. and Gea, H.C., Topology optimization with design-dependent pressure loading, J. Structural and Multidisciplinary Optimization, 38(6) (2009) 535-543.

[12] Gao, X. and Zhao, K. and Gu, Y., Topology optimization with design-dependent loads by level set approach, In: 10th AIAA/ISSMO Multidisciplinary Analysis and Optimization Conference, (2004) 4526.

[13] Li, C. and Xu, C. and Gui, C. and Fox, M.D., Distance regularized level set evolution and its application to image segmentation, J. IEEE Transactions on Image Processing, 19(12) (2010) 3243-3254.

[14] Xia, Q. and Wang, M.Y. and Shi, T., Topology optimization with pressure load through a level set method, J. Computer Methods in Applied Mechanics and Engineering, 283 (2015) 177–195.

[15] Bourdin, B. and Chambolle, A., Design-dependent loads in topology optimization, ESAIM: Control, Optimisation and Calculus of Variations., 9 (2003) 19-48.

[16] Panganiban, H. and Jang, G.W. and Chung, T.J., Topology optimization of pressure-actuated compliant mechanisms, ESAIM: Control, Optimisation and Calculus of Variations., 46(3) (2010) 238-246

[17] Sigmund, O. and Clausen, P.M., Topology optimization using a mixed formulation: An alternative way to solve pressure load problems, J. Computer Methods in Applied Mechanics and Engineering, 196 (13-16) (2007) 1874-1889.

[18] Vasista, S. and Tong, L.,Design and testing of pressurized cellular planar morphing structures, AIAA journal, 50(6) (2012) 1328-1338.

[19] Zhang, H. and Zhang, X. and Liu, S.T., A new boundary search scheme for topology optimization of continuum structures with design-dependent loads, J. Structural and Multidisciplinary Optimization, 37(2) (2008) 121-129.

[20] Wang, C. and Zhao, M. and Ge, T., Structural topology optimization with design-dependent pressure loads., J. Structural and Multidisciplinary

Optimization, 53(5) (2016) 1005-1018.

[21] Picelli, R. and Neofytou, A. and Kim, H.A., Structural topology optimization with design-dependent pressure loads., Topology optimization for design-dependent hydrostatic pressure loading via the level-set method, 60(4) (2019) 1313-1326.

[22] Zienkiewicz, O.C. and Taylor, R.L., The Finite Element Method for Solid and Structural Mechanics, Butterworth-heinemann, 2005.

[23] Kumar, P. and Frouws, J.S. and Langelaar, M., Topology Optimization of Fluidic Pressure Loaded Structures and Compliant Mechanisms using the Darcy Method, Springer: Structural and Multidisciplinary Optimization, 61 (2020) 1637-1655.

[24] Hübner, D. and Rohan, E. and Lukeš, V. and Stingl, M., Optimization of the porous material described by the Biot model, Elsevier, International Journal of Solids and Structures, 156-157 (2019) 216-233.

[25] Allaire,G. and Bonnetier,E. and Francfort,G. and Jouve,F., Shape optimization by homogenization method, Springer-Verlag. J. Numer. Math., 76 (1997) 27-68.

[26] Murat,F., Contre-exemples pour divers problèmes où le controle intervient dans les coefficients, Ann. Mat. Pura Appl., 112 (1997) 49-68.

[27] Pantz,O. and Trabelsi,K., A post-treatment of the homogenization method for shape optimization, SIAM Journal on Control and Optimization, 47(3) (2008) 1380–1398.

[28] Geoffrey-Donders, P., Homogenization method for topology optimization of structures built with lattice materials, PhD thesis, Universit´é Paris Saclay (COmUE), 2018.

[29] Jobic, Y. and Kumar, P. and Topin, F. and Occelli, R., Transport properties of solid foams having circular strut cross section using pore scale numerical simulations, Heat Mass Transfer, 54 (2018) 2351–2370.

[30] Batchelor, G., An introduction to fluid dynamics, Cambridge university press, 2000.

[31] Neuber, H., Theory of notch stresses: principles for exact calculation of strength with reference to structural form and material, USAEC Office of Technical Information, (1961) 4547.

[32] Abad, K.M.E. and Khanoki, A.S. and Pasini, D.F., Fatigue design of lattice materials via computational mechanics: Application to lattices with

smooth transitions in cell geometry, International Journal of Fatigue, 47 (2013) 126-136.

[33] Vigdergauz, S., Energy-minimizing inclusions in a planar elastic structure with macroisotropy, Structural optimization, 17(2-3) (2013) 104-112.

[34] Allaire, G., Shape Optimization by the Homogenization Method, Springer, Applied Mathematical Sciences, 146 (2002).

[35] Hashin, Z. and Shtrikman, S., A variational approach to the theory of the elastic behaviour of multiphase materials, Journal of the Mechanics and Physics of Solids, 11(2) (1963) 127-140.

[36] Allaire, G., Conception optimale de structures, Springer-Verlag Berlin Heidelberg, Applied Mathematical Sciences, 19(2) (2000) 58 (2007).

[37] Bendsoe, M. and Diaz, A. and Kikuchi, N., Topology and generalized layout optimization of structures, In: Topology Optimization of Structures, Nato ASI Series E, Bendsoe M., et al. (eds), (Kluwer, Dordrecht, 1993) 159-205.

[38] Jog, C. and Haber, R. and Bendsoe, M., A displacement-based topology design method with self-adaptive layered materials. In: Topology design of structures, Nato ASI Series E, Bendsoe M., et al. (eds.), Int. Journal for Numerical Methods in Engineering, (Kluwer, Dordrecht , 1993) 219-238.

[39] Jog, C. and Haber, R. and Bendsoe, M., Topology design with optimized, self-adaptative materials, Int. Journal for Numerical Methods in Engineering, 39(10) (2003) 1667-1694.

[40] Bendsoe, M.P. and Kikuchi, N., Generating optimal topologies in structural design using a homogenization method, Comput. Methods Appl. Mech. Engrg, 71(2) (1988) 197-224.

[41] Allaire, G. and Kohn, R.V., Optimal design for minimum weight and compliance in plane stress using extremal microstructures, Europ. J. Mech. A/Solids, 12(6) (1993) 839-878.

[42] Suzuki, K. and Kikuchi, N., A homogenization method for shape and topology optimization, Comp. Meth. Appl. Mech. Eng., 93 (1991) 291-318.

[43] Hecht, F., J. Math. Anal. Appl., New development in freefem++, J. Numerical Mathematics, (2012).

[44] Chen, B.C. and Kikuchi, N., Topology optimization with design-dependent loads. Finite elements in analysis and design, ESAIM: Control, Optimisation and Calculus of Variations., 37(1) (2001) 57-70.

[45] Céa, J., Conception optimale ou identification de formes, calcul rapide de la dérivée directionnelle de la fonction coût, ESAIM: Mathematical Modelling and Numerical Analysis, 30(6) (1986) 371-402.